

Research



Cite this article: Maiden MD, Hoefler, MA.
2016 Modulations of viscous fluid conduit
periodic waves. *Proc. R. Soc. A* **472**: 20160533.
<http://dx.doi.org/10.1098/rspa.2016.0533>

Received: 1 July 2016

Accepted: 14 November 2016

Subject Areas:

applied mathematics

Keywords:

Whitham theory, nonlinear Schrödinger
equation, modulational instability,
envelope solitons

Author for correspondence:

M. D. Maiden

e-mail: michelle.maiden@colorado.edu

M. D. Maiden and M. A. Hoefler

Department of Applied Mathematics, University of Colorado,
Boulder, CO, USA

 MDM, 0000-0003-1294-0289; MAH, 0000-0001-5883-6562

Modulated periodic interfacial waves along a conduit of viscous liquid are explored using nonlinear wave modulation theory and numerical methods. Large-amplitude periodic-wave modulation (Whitham) theory does not require integrability of the underlying model equation, yet often either integrable equations are studied or the full extent of Whitham theory is not developed. Periodic wave solutions of the nonlinear, dispersive, non-integrable conduit equation are characterized by their wavenumber and amplitude. In the weakly nonlinear regime, both the defocusing and focusing variants of the nonlinear Schrödinger (NLS) equation are derived, depending on the carrier wavenumber. Dark and bright envelope solitons are found to persist in long-time numerical solutions of the conduit equation, providing numerical evidence for the existence of strongly nonlinear, large-amplitude envelope solitons. Due to non-convex dispersion, modulational instability for periodic waves above a critical wavenumber is predicted and observed. In the large-amplitude regime, structural properties of the Whitham modulation equations are computed, including strict hyperbolicity, genuine nonlinearity and linear degeneracy. Bifurcating from the NLS critical wavenumber at zero amplitude is an amplitude-dependent elliptic region for the Whitham equations within which a maximally unstable periodic wave is identified. The viscous fluid conduit system is a mathematically tractable, experimentally viable model system for wide-ranging nonlinear, dispersive wave dynamics.

1. Introduction

Nonlinear wave modulation is a major mathematical component of the description of dispersive hydrodynamic phenomena. Dispersive hydrodynamics encompass

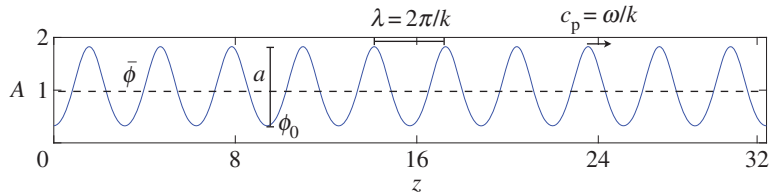


Figure 1. A computed periodic wave solution to the conduit equation with wavenumber $k = 2$, amplitude $a = 1.5$ and unit mean. (Online version in colour.)

the study of fluid-like media where dissipative effects are weak compared to dispersion [1]. Solitary waves and dispersive shock waves (DSWs) are typical coherent structures. Model equations include the integrable Korteweg–de Vries (KdV) and nonlinear Schrödinger (NLS) equations as well as non-integrable counterparts that are important for applications to superfluids, geophysical fluids and laser light. Modulation theory assumes the existence of a multi-parameter family of nonlinear, periodic travelling wave solutions whose parameters change slowly relative to the wavelength and period of the periodic solution under perturbation. Such variation is described by modulation equations. In the weakly nonlinear regime, the NLS equation is a universal model for the slowly varying envelope and phase, incorporating both cubic nonlinearity and dispersion. In the large-amplitude regime, the Whitham equations [2] describe slow modulations of the wave's mean, amplitude and wavenumber. At leading order, they are a dispersionless system of quasi-linear equations.

In this paper, we investigate nonlinear wave modulations in both the weakly nonlinear and large-amplitude regimes for the dimensionless conduit equation

$$A_t + (A^2)_z - (A^2(A^{-1}A_t)_z)_z = 0. \quad (1.1)$$

This equation approximately models the evolution of the circular interface, with cross-sectional area A at time t and vertical spatial coordinate z , separating a light, viscous fluid rising buoyantly through a heavier, more viscous, miscible fluid at small Reynolds numbers [3,4]. Our motivation for studying equation (1.1) is twofold. First, the conduit equation is not integrable [5], so there are mathematical challenges in analysing its rich variety of nonlinear wave features. Second, equation (1.1) is an accurate model of viscous fluid conduit interfacial waves where hallmark experiments have been performed on solitary waves [6–8], their interactions [3,9,10] and DSWs [11]. We believe the conduit system is an ideal model for the study of a broad range of dispersive hydrodynamic phenomena.

Indeed, in this work, we elucidate additional nonlinear wave phenomena predicted by equation (1.1) by analysing its weakly nonlinear, NLS reduction, the structural properties of the large-amplitude Whitham equations, and numerical simulations. An example of a non-modulated periodic wave is shown in figure 1 that defines the wave's mean $\bar{\phi}$, amplitude a , wavenumber k , minimum ϕ_0 , and phase velocity $c_p = \omega/k$ (ω is the wave's frequency). We identify persistent bright and dark envelope soliton solutions in both the weakly nonlinear, NLS regime and the large-amplitude, strongly nonlinear regime. The quasi-linear Whitham equations are analysed asymptotically and with numerical computation. Regions in parameter space of strict hyperbolicity, ellipticity and linear degeneracy are identified. The elliptic regime corresponds to modulationally unstable periodic waves and a maximally unstable wave is identified.

(a) Background on viscous fluid conduits

Conduits generated by the low Reynolds number, buoyant dynamics of two miscible fluids with differing densities and viscosities were first studied in the context of geological and geophysical processes [12]. A system of equations describing the dynamics of melted rock within a solid rock matrix was derived by treating molten rock and its solid, porous surroundings as two fluids with a

large density and viscosity difference [13]. Under appropriate assumptions, the family of magma equations

$$\varphi_t + (\varphi^n)_x - (\varphi^n(\varphi^{-m}\varphi_t)_x)_x = 0, \quad (1.2)$$

describing the evolution of the volume fraction φ of molten rock, can be derived [14,15]. There are two constitutive model parameters (n, m) that relate the porosity of the rock matrix to its permeability and viscosity, respectively. Physical values of the parameters are $2 \leq n \leq 5, 0 \leq m \leq 1$. The conduit equation (1.1) happens to coincide with the magma equation (1.2) when $(n, m) = (2, 1)$ [3]. For this reason, viscous fluid conduits were utilized as a laboratory model of magma dynamics. The conduit equation can be derived directly from the Stokes equations for two viscous fluids under a long-wave, high-viscosity contrast assumption [4]. Viscous fluid conduits, contrary to magma, are easily accessible in a laboratory setting, typically with a sugar solution or glycerine for the exterior fluid, and a dyed, diluted version of the same for the interior fluid [3,6,9,11].

Early experiments primarily explored the development of the conduit itself, which results in a diapir followed by a periodic wavetrain [6,12]. Solitary waves in an established conduit have also been extensively studied, including their amplitude–speed relation, interactions and fluid transport properties [3,6–8,10]. Experiments have also shown that interactions between solitons are nearly elastic, with a phase shift the primary quantifiable change [8,10]. Furthermore, soliton interaction geometries predicted by Lax for the KdV equation [16] were observed and agreed well with numerical simulations [10]. This is particularly notable because the Lax categories persisted into the large-amplitude regime, although unlike KdV, the short-wavelength behaviour of conduit dispersion is bounded, akin to the Benjamin–Bona–Mahoney (BBM) equation [10]. Recently, dispersive shock waves were observed, yielding good agreement with predictions from Whitham averaging theory [11]. The accompanying observations of soliton–DSW interaction suggest a high degree of coherence, i.e. the sustenance of dissipationless/dispersive hydrodynamics over long spatial and temporal time scales. It is for this reason that we further investigate modulations of periodic conduit waves.

(b) Properties of the conduit equation

To fully describe the two-fluid interface of the conduit system, one can consider the full Navier–Stokes equations with boundary conditions along a moving, free interface. However, in the low Reynolds number, small interfacial slope, long-wave regime, a balance between the viscous stress force of the exterior fluid and the buoyancy force acting on the interior fluid leads to the asymptotically resolved conduit equation (1.1) with no amplitude assumption [4,6]. The force balance is achieved with small interfacial slopes on the order of the square root of the ratio of the interior to exterior fluid viscosities.

The conduit equation (1.1) has been studied since the 1980s and is known to have exactly two conservation laws [17,18]:

$$\text{and} \quad \left. \begin{aligned} A_t + (A^2 - A^2(A^{-1}A_t)_z)_z &= 0 \\ \left(\frac{1}{A} + \frac{A_z^2}{A^2} \right)_t + \left(\frac{A_{tz}}{A} - \frac{A_z A_t}{A^2} - 2 \ln A \right)_z &= 0. \end{aligned} \right\} \quad (1.3)$$

The conduit equation itself corresponds to conservation of mass and obeys the scaling invariance

$$\tilde{A} = \frac{A}{A_0}, \quad \tilde{z} = A_0^{-1/2} z \quad \text{and} \quad \tilde{t} = A_0^{1/2} t. \quad (1.4)$$

The linearization of the conduit equation upon a unit area background admits trigonometric travelling wave solutions subject to the frequency dispersion relation

$$\omega_0(k) = \frac{2k}{1+k^2}, \quad (1.5)$$

with wavenumber k , similar to the bounded dispersion of the BBM equation. This leads to the linear phase c_p and group c_g velocities

$$c_p(k) = \frac{\omega_0(k)}{k} = \frac{2}{1+k^2} \quad \text{and} \quad c_g(k) = \omega'_0(k) = \frac{2(1-k^2)}{1+k^2}. \quad (1.6)$$

Note that $c_g < c_p$ for $k > 0$. While the phase velocity is always positive, the group velocity is negative for $k > 1$. Failure of the Painlevé test suggests that the conduit equation is not completely integrable [5]. The conduit equation is globally well-posed for initial data $A(\cdot, 0) - 1 \in H^1(\mathbb{R})$, with $A(z, 0)$ physically relevant data bounded away from zero in order to avoid the singularity [19].

Solitary waves have been studied numerically for the more general magma equation (1.2), where it has been found that they exhibit near-elastic interactions resulting in a phase shift and a physically negligible dispersive tail [10,20,21]. The asymptotic stability of solitary waves has also been proved [22]. General (unmodulated) periodic wave solutions have been found, and an implicit dispersion relation has been computed for these waves [6]. In the long-wavelength, small-amplitude regime, the conduit equation reduces to KdV [23]. However, the fact that solitary waves exhibit KdV-like interaction behaviour including almost elastic interactions, the three Lax interaction categories [10] and coherent interactions with DSWs [11], all for strongly nonlinear, large-amplitude solitary waves is notable.

There have been several works that apply Whitham modulation theory to the magma equations (1.2). Marchant & Smyth [24] considered equation (1.2) with $(n, m) = (3, 0)$, describing DSWs and some structural properties of the Whitham equations. Modulations of periodic travelling waves in the magma equation (1.2) and a generalization of it were investigated in the weakly nonlinear, KdV regime [25]. Modulated periodic waves in the form of DSWs were investigated for the entire family of magma equations (1.2) in [26]. This work differs from previous studies by concentrating on the case $(n, m) = (2, 1)$ for the conduit equation, identifying new coherent structures (envelope solitons) and determining structural properties of the associated Whitham equations (hyperbolicity, ellipticity, linear degeneracy).

(c) Outline of this work

The paper is organized as follows. Periodic travelling wave solutions to the conduit equation are studied in §2 both numerically and asymptotically in the weakly nonlinear regime. In §3, we consider weakly nonlinear periodic wave modulations and include long-wave dispersion to derive the NLS equation. By an appropriate choice of the periodic travelling wave's wavenumber, both the focusing and defocusing variants of the NLS equation are possible. We numerically demonstrate the persistence of large-amplitude dark and bright envelope solitary wave solutions in the full conduit equation. In §4, we analyse modulated periodic waves of arbitrary amplitude via the conduit Whitham modulation equations. A weakly nonlinear analysis and direct numerical computation are used to determine structural properties of the Whitham equations including hyperbolicity or ellipticity and genuine nonlinearity or linear degeneracy. Consequences for the stability of periodic waves are examined. The manuscript is concluded with a discussion of the implications of this work in §5.

2. Periodic travelling wave solutions

We seek periodic travelling wave solutions to equation (1.1) in the form $A(z, t) = \phi(\theta)$, $\theta = kz - \omega t$, $\phi(\theta + 2\pi) = \phi(\theta)$ for $\theta \in \mathbb{R}$. Inserting this ansatz into equation (1.1) yields

$$-\omega\phi' + k(\phi^2)' + \omega k^2(\phi^2(\phi^{-1}\phi'))' = 0. \quad (2.1)$$

Integrating twice results in

$$(\phi')^2 = g(\phi) \equiv -\frac{2}{k^2}\phi - \frac{2}{\omega k}\phi^2 \ln \phi + A + B\phi^2, \quad (2.2)$$

where A and B are real integration constants.

The above equation exhibits at most three real roots [26]. When there are three distinct roots, a periodic solution oscillates between the largest two. The solution can therefore be parametrized by three independent variables. Defining the wave minimum ϕ_0 according to $\phi_0 = \min_{\theta} \phi(\theta)$, we use the following physical parametrization:

$$\left. \begin{aligned} \text{wavenumber: } & k, \\ \text{wave amplitude: } & a = \max_{\theta \in [0, \pi]} \phi(\theta) - \phi_0 \\ \text{and} \quad \text{wave mean: } & \bar{\phi} \equiv \frac{1}{\pi} \int_0^{\pi} \phi(\theta) \, d\theta = \frac{1}{\pi} \int_{\phi_0}^{\phi_0+a} \frac{\phi \, d\phi}{\sqrt{g(\phi)}} \end{aligned} \right\} \quad (2.3)$$

The requirement that ϕ is 2π -periodic is enforced through

$$\pi = \int_0^{\pi} d\theta = \int_{\phi_0}^{\phi_0+a} \frac{d\phi}{\sqrt{g(\phi)}}, \quad (2.4)$$

where, in (2.3) and (2.4), we have used the even symmetry of solutions to equation (2.2). Given $(k, a, \bar{\phi})$, the relations (2.3) and (2.4) determine the wave frequency $\omega = \omega(k, a, \bar{\phi})$ and the wave minimum $\phi_0 = \phi_0(k, a, \bar{\phi})$. The extrema requirements $g(\phi_0) = g(\phi_0 + a) = 0$ determine A and B from equation (2.2).

Owing to the scaling invariance equation (1.4), the wave mean can be scaled to unity. This implies that only $\omega(k, a, 1)$ and $\phi_0(k, a, 1)$ need be determined. Then the general cases follow according to

$$\omega(k, a, \bar{\phi}) = \bar{\phi}^{1/2} \omega(\bar{\phi}^{1/2} k, \bar{\phi}^{-1} a, 1) \quad \text{and} \quad \phi_0(k, a, \bar{\phi}) = \bar{\phi} \phi_0(\bar{\phi}^{1/2} k, \bar{\phi}^{-1} a, 1). \quad (2.5)$$

We therefore define the unit-mean dispersion and wave solution according to

$$\tilde{\omega}(\tilde{k}, \tilde{a}) = \omega(\tilde{k}, \tilde{a}, 1) \quad \text{and} \quad \tilde{\phi}(\theta; \tilde{k}, \tilde{a}) = \phi(\theta; \tilde{k}, \tilde{a}, 1). \quad (2.6)$$

We will use the variables $(\tilde{\phi}, \tilde{\omega}, \tilde{k}, \tilde{a})$ whenever we are assuming a unit mean solution.

(a) Stokes expansion

We can obtain approximate periodic travelling wave solutions in the weakly nonlinear regime via the Stokes wave expansion [27]:

$$\tilde{\phi} = 1 + \varepsilon \tilde{\phi}_1 + \varepsilon^2 \tilde{\phi}_2 + \varepsilon^3 \tilde{\phi}_3 + \dots \quad (2.7)$$

and

$$\tilde{\omega} = \tilde{\omega}_0 + \varepsilon^2 \tilde{\omega}_2 + \dots, \quad (2.8)$$

where $0 < \varepsilon \ll 1$ is an amplitude scale. Inserting this ansatz into equation (2.1), equating like coefficients in ε and enforcing solvability conditions yield the approximate solution

$$\tilde{\phi}_1(\theta) = \cos \theta, \quad \tilde{\omega}_0(k) = \frac{2\tilde{k}}{1 + \tilde{k}^2}, \quad \tilde{\phi}_2(\theta) = \frac{1}{6\tilde{k}\tilde{\omega}_0} \cos 2\theta \quad \text{and} \quad \tilde{\omega}_2(\tilde{k}) = \frac{1 - 8\tilde{k}^2}{48\tilde{k}(1 + \tilde{k}^2)}, \quad (2.9)$$

where $\tilde{\omega}_0$ is the unit mean linear dispersion relation (1.5). Setting the amplitude $\tilde{a} = 2\varepsilon$, the approximate periodic wave solution is

$$\tilde{\phi}(\theta, \tilde{k}, \tilde{a}) = 1 + \frac{\tilde{a}}{2} \cos \theta + \frac{\tilde{a}^2(1 + \tilde{k}^2)}{48\tilde{k}^2} \cos 2\theta + \mathcal{O}(\tilde{a}^3) \quad (2.10)$$

and

$$\tilde{\omega}(\tilde{k}, \tilde{a}) = \frac{2\tilde{k}}{1 + \tilde{k}^2} + \tilde{a}^2 \frac{1 - 8\tilde{k}^2}{48\tilde{k}(1 + \tilde{k}^2)} + \mathcal{O}(\tilde{a}^3). \quad (2.11)$$

In figure 2, this solution is compared to numerically computed periodic waves (numerical methods are described in appendix A(a)). The frequency and wave profile of the Stokes expansion accurately describe some periodic conduit waves, even for $\mathcal{O}(1)$ amplitudes, provided the

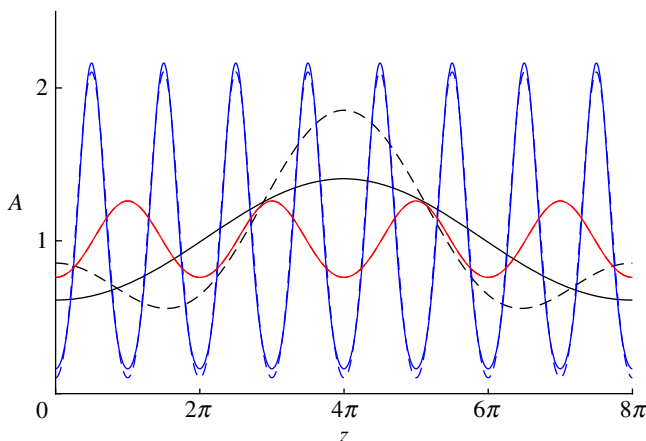


Figure 2. Comparison of the Stokes wave expansion solution (dashed lines) to the numerically computed solution (solid lines) for three different waves with unit mean. Here (\tilde{k}, \tilde{a}) are $(\frac{1}{4}, 1)$ (black), $(2, 2)$ (blue) and $(1, 0.5)$ (red). Note that the approximate and numerical solutions for $(\tilde{k}, \tilde{a}) = (1, 0.5)$ are essentially indistinguishable. (Online version in colour.)

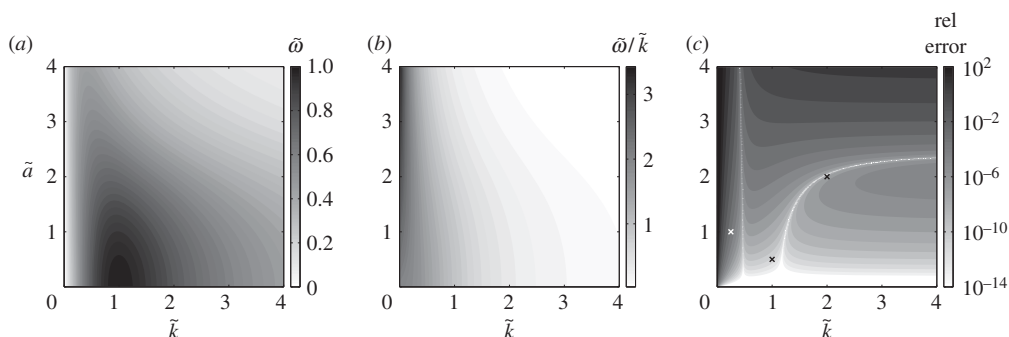


Figure 3. (a) Contour plot of numerically computed dispersion relation. (b) Numerically computed phase velocity. (c) Relative error between numerically computed dispersion $\tilde{\omega}(\tilde{k}, \tilde{a})$ and approximate dispersion $\tilde{\omega}_0(\tilde{k}) + \tilde{a}^2 \tilde{\omega}_2(\tilde{k})$. Markers (\times) correspond to waves plotted in figure 2.

wavenumber is appropriately chosen. However, even at moderately small wavenumbers, the expansion rapidly breaks down. This is quantified in figure 3. Figure 3*a,b* shows the dispersion and phase velocities for numerically computed periodic waves, and figure 3*c* compares the full, nonlinear dispersion $\tilde{\omega}(\tilde{k}, \tilde{a})$ to $\tilde{\omega}_0(\tilde{k}) + \tilde{a}^2 \tilde{\omega}_2(\tilde{k})$. The dispersion relation agrees exceedingly well for $\tilde{k} > 1$ and $\tilde{a} \lesssim 1$, but deviates for larger amplitudes and wavenumbers less than 0.5.

Of interest is that the approximate solution (2.10) can result in an unphysical, negative conduit cross-sectional area. The minimum of the approximate solution $\tilde{\phi}(\theta)$ occurs when $\theta = \pi$. Equating the minimum to zero, we find that physical, positive values for approximate $\tilde{\phi}$ are restricted to $\tilde{a} < a_0$, where $a_0 = 4(3 - \sqrt{6}) \approx 2.20$, which is well beyond our assumption of small amplitude $0 < \tilde{a} \ll 1$.

3. Weakly nonlinear, dispersive modulations

The aim of this section is to describe wave modulation in the weakly nonlinear, dispersive regime. The approximate NLS equation is found using multiple scales in appendix B by seeking a solution

in the form [2,28]

$$A(z, t) = 1 + \varepsilon[\sqrt{n}B e^{i\theta} + \text{c.c.}] + \varepsilon^2 \left[\frac{nB^2}{3\tilde{k}\tilde{\omega}_0} e^{2i\theta} + \text{c.c.} + M \right] + \mathcal{O}(\varepsilon^3) \quad (3.1)$$

and

$$M = \frac{(3\tilde{k} - 1)(1 + \tilde{k}^2)}{\tilde{k}^2(\tilde{k}^2 + 3)} n|B|^2, \quad n(\tilde{k}) = \frac{3 + 5\tilde{k}^2 + 8\tilde{k}^4}{3\tilde{k}(\tilde{k}^2 + 1)(\tilde{k}^2 + 3)}$$

where 'c.c.' denotes complex conjugate and ε is an amplitude scale. By introducing the standard, scaled coordinate system

$$\tau = \varepsilon^2 t \quad \text{and} \quad \zeta = \frac{\varepsilon}{\sqrt{|\tilde{\omega}_0''|}} (z - \tilde{\omega}_0' t), \quad (3.2)$$

we obtain the NLS equation for the complex envelope $B(\zeta, \tau)$

$$iB_\tau + \frac{\sigma}{2} B_{\zeta\zeta} + |B|^2 B = 0, \quad (3.3)$$

where $\sigma = \text{sgn} \tilde{\omega}_0''(\tilde{k})$ denotes the dispersion curvature. As

$$\tilde{\omega}_0''(\tilde{k}) = \frac{4\tilde{k}(\tilde{k}^2 - 3)}{(1 + \tilde{k}^2)^3},$$

the NLS equation (3.3) is defocusing when $0 < \tilde{k} < \sqrt{3}$, and focusing for $\tilde{k} > \sqrt{3}$. This result effectively splits periodic wave solutions of the conduit equation into two regimes. For the defocusing case, weakly nonlinear periodic waves are modulationally stable, and dark envelope solitons are predicted, which, when combined with the ansatz (3.1), take the form (e.g. [28])

$$B(\zeta, \tau) = e^{i\tau + i\psi_0} [i \cos \alpha + \sin \alpha \tanh[\sin \alpha (\zeta - \cos \alpha \tau - \zeta_0)]], \quad (3.4)$$

with arbitrary, real constants ζ_0 , ψ_0 and α , where $0 < \alpha \leq \pi/2$ is the phase jump across the soliton. The grey soliton reduces to a black soliton when $\alpha = \pi/2$.

For the focusing case, periodic waves are modulationally unstable [2,29]. Bright envelope solitons for the NLS equation exist, which have the form

$$B(\zeta, \tau) = e^{i\tau/2 + i\Theta_0} \text{sech}(\zeta - \zeta_0), \quad (3.5)$$

where ζ_0 and Θ_0 are arbitrary, real constants. To validate these approximate solutions, we numerically simulate the conduit equation (1.1) with envelope soliton initial conditions (3.1) and (3.4) or (3.1) and (3.5), depicted in figure 4*a,b*. In figure 4*a*, a black soliton is observed to coherently propagate, maintaining essentially the same shape. The NLS approximation is asymptotically valid up to times $t = \mathcal{O}(1/\varepsilon^2)$. For the simulation in figure 4*a*, $\varepsilon = \tilde{a}/4 = 0.05$ so that $1/\varepsilon^2 = 400$. The black envelope soliton shows no sign of instability over times up to $t = 1000$. Figure 4*b* shows the long-time evolution of an envelope bright soliton. The envelope appears to steepen and become peaked by $t = 1000$ but otherwise maintain its essential structure. The observed speeds of propagation of the black and bright solitons are 0.0002 and -0.1589 very close to the predicted group velocities 0 and -0.16 , respectively.

We also numerically studied the large-amplitude regime with dark and bright envelope soliton initial conditions. Figure 5*a* shows the numerical evolution of dark envelope soliton initial data (3.1), (3.4) for $\tilde{a} = 1.6$, $\tilde{k} = 1$, $\alpha = \pi/2$. The initial data apparently breaks up into three coherent structures. Two shallow amplitude modulations propagate in opposite directions and a large-amplitude dip propagates very slowly. To verify the coherence of this large-amplitude structure, we isolate it from the fast nonlinear waves by extracting the solution at $t = 750$ over the truncated domain $z \in [100, 175]$ and use this as an initial condition for the conduit equation. Additional periods of the unmodulated wave were prepended to the profile in order to increase the spatial domain. The evolution is shown in figure 5*b*, displaying a remarkable coherence and persistence out to $t = 1000$.

Figure 6*a* depicts the evolution of bright envelope soliton initial conditions with $\tilde{a} = 0.6$, $\tilde{k} = 3$. The initial envelope appears to split into two coherent bright envelope structures and

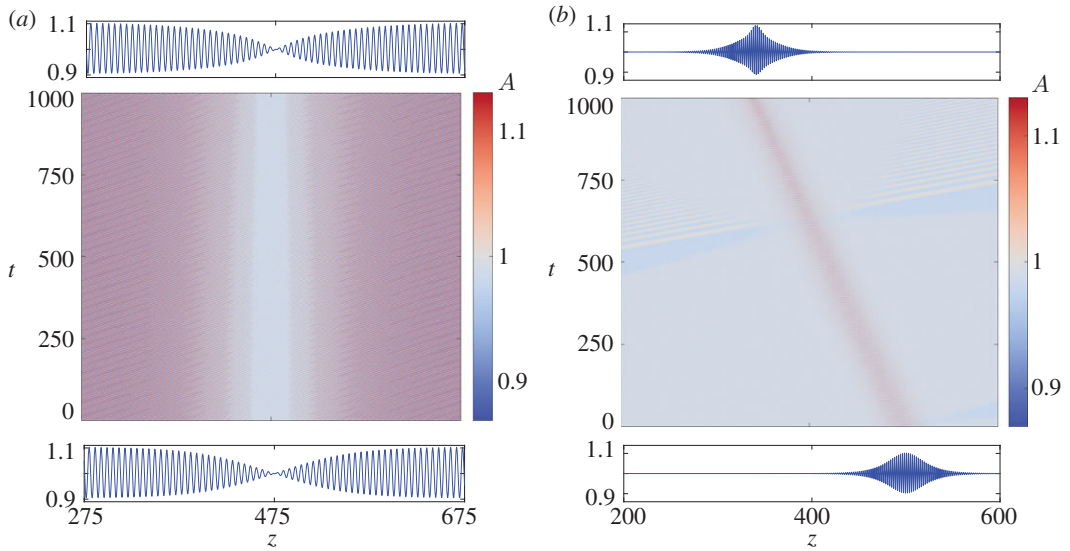


Figure 4. Evolution of weakly nonlinear envelope soliton initial conditions for the conduit equation (1.1). (a) Approximate black soliton initial condition (3.4) with $\tilde{a} = 0.2, \tilde{k} = 1, \alpha = \pi/2$. (b) Approximate bright soliton initial condition (3.5) with $\tilde{a} = 0.2, \tilde{k} = 3$. (Online version in colour.)

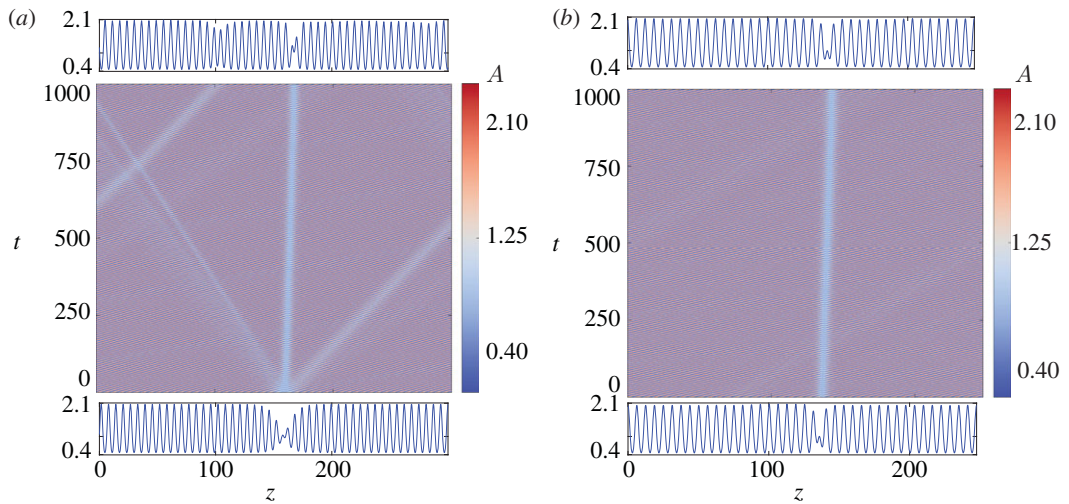


Figure 5. Evolution of large-amplitude dark envelope soliton initial conditions for the conduit equation (1.1). (a) Approximate black soliton initial condition (3.4) with $\tilde{a} = 1.6, \tilde{k} = 1, \alpha = \pi/2$ breaking up into multiple coherent ‘dark’ wave structures. (b) The large amplitude dark structure from (a) is isolated and evolved, maintaining its coherence. (Online version in colour.)

small-amplitude dispersive radiation. The large-amplitude wave is extracted from the solution at $t = 1000$ over the truncated domain $z \in [350, 360]$ and superimposed on a unit background and then used as a new initial condition for the conduit equation. The result is shown in figure 6b that shows the persistence of a large-amplitude envelope structure accompanied by the emission of small-amplitude dispersive radiation.

These results reflect the fact that the NLS approximation models the envelope of a weakly nonlinear, dispersive carrier wave. Yet numerical evolution of large-amplitude initial data present

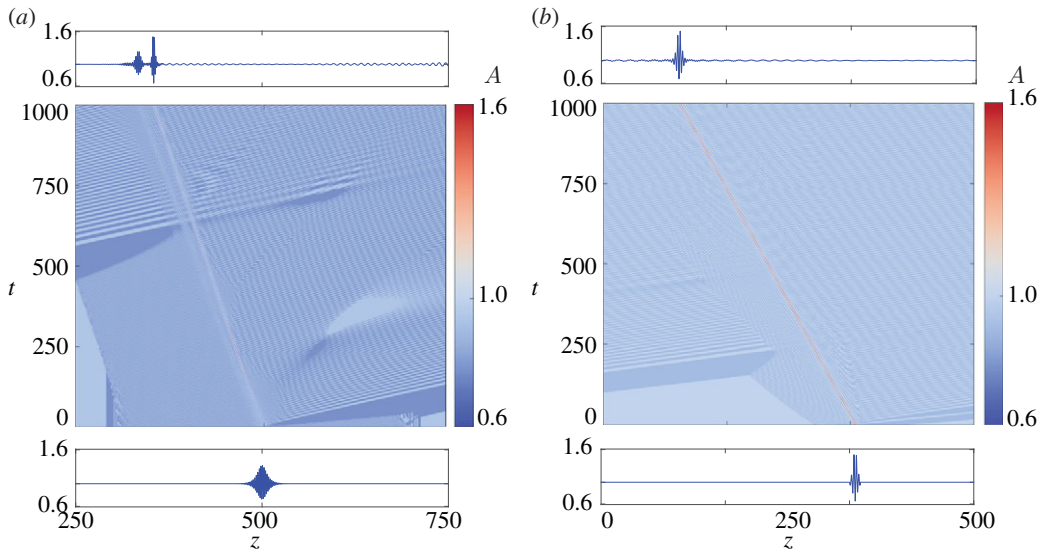


Figure 6. Evolution of large-amplitude bright envelope soliton initial conditions for the conduit equation (1.1). (a) Approximate bright soliton initial condition (3.4) with $\tilde{a} = 0.6$, $\tilde{k} = 3$ breaking up into two coherent ‘bright’ wave structures and small-amplitude dispersive radiation. (b) The largest amplitude bright structure from (a) is isolated and evolved, maintaining its coherence. (Online version in colour.)

intriguing coherent structures deserving of further study. We now turn to the Whitham equations for an asymptotic description of nonlinear wave modulations in the moderate- to large-amplitude regime. However, the trade-off for using these quasi-linear equations is their lack of dispersion at the first order of approximation; consequently, they cannot describe envelope solitons.

4. Whitham equations

To describe modulated, large-amplitude periodic waves, we appeal to the Whitham modulation equations. Whitham’s original formulation invoked averaged conservation laws [30], later shown to be equivalent to a perturbative, multiple-scales reduction [31]. For completeness, we have implemented both approaches in appendix C. For this, we seek modulations of an arbitrary amplitude, 2π -periodic, travelling wave solution ϕ to equation (1.1) (see §2). As we will incorporate only the leading-order Whitham equations, the large parameter $1/\varepsilon$ here corresponds to the time scale of their validity. Note that the lack of an amplitude restriction in leading order Whitham modulation theory is at the expense of a shorter time scale of validity relative to the $\mathcal{O}(1/\varepsilon^2)$ time scale for the small-amplitude NLS modulation (3.3).

It is convenient to express the Whitham equations in the conservative form

$$\mathcal{P}_t + \mathcal{Q}_z = 0, \quad \mathcal{P} = \begin{bmatrix} \bar{\phi} \\ I_1 \\ k \end{bmatrix} \quad \text{and} \quad \mathcal{Q} = \begin{bmatrix} I_2 \\ I_3 \\ \omega \end{bmatrix}, \quad (4.1)$$

introducing the averaging integrals

$$I_1 = \bar{\phi}^{-1} + k^2 \overline{g(\phi)/\phi^2}, \quad I_2 = \bar{\phi}^2 - 2k\omega \overline{g(\phi)} \quad \text{and} \quad I_3 = -2\overline{\ln \phi}. \quad (4.2)$$

We recall the defining ordinary differential equation (ODE) $\phi^2 = g(\phi)$ (2.2) and use the notation

$$\bar{f} = \frac{1}{2\pi} \int_0^{2\pi} f(\theta) d\theta.$$

The density \mathcal{P} and flux \mathcal{Q} can be expanded in terms of the modulation variables $\mathbf{q} = (k, a, \bar{\phi})^T$ to obtain the quasi-linear form of the Whitham equations

$$\mathbf{q}_t + \mathcal{A}\mathbf{q}_z = 0, \quad (4.3)$$

where

$$\mathcal{A} = \left(\frac{\partial \mathcal{P}}{\partial \mathbf{q}} \right)^{-1} \frac{\partial \mathcal{Q}}{\partial \mathbf{q}} = \begin{bmatrix} \frac{\omega_k}{I_{3,k} - I_{1,k}\omega_k - I_{2,k}I_{1,\bar{\phi}}} & \frac{\omega_a}{I_{3,a} - I_{1,k}\omega_a - I_{2,a}I_{1,\bar{\phi}}} & \frac{\omega_{\bar{\phi}}}{I_{3,\bar{\phi}} - I_{1,k}\omega_{\bar{\phi}} - I_{2,\bar{\phi}}I_{1,\bar{\phi}}} \\ I_{1,a} & I_{1,a} & I_{1,a} \\ I_{2,k} & I_{2,a} & I_{2,\bar{\phi}} \end{bmatrix}. \quad (4.4)$$

This non-conservative form of the Whitham equations is only valid where the matrix $\partial \mathcal{P} / \partial \mathbf{q}$ is invertible.

The scaling invariance (1.4) can be used so that the dependence on $\bar{\phi}$ in the Whitham equations is explicit and the averaging integrals need be computed only over the scaled variables \tilde{k} and \tilde{a} . Then the integrals (4.2) can be written

$$I_1 = \frac{\tilde{I}_1}{\bar{\phi}}, \quad I_2 = \bar{\phi}^2 \tilde{I}_2 \quad \text{and} \quad I_3 = \tilde{I}_3 - 2 \ln \bar{\phi}, \quad (4.5)$$

where $\tilde{I}_i = \tilde{I}_i(\tilde{k}, \tilde{a})$, $i = 1, 2, 3$. Therefore, computation of the averaging integrals is only required for (\tilde{k}, \tilde{a}) . The Whitham equations in the scaled variables $\tilde{\mathbf{q}} = (\tilde{k}, \tilde{a}, \bar{\phi})$ are

$$\tilde{\mathbf{q}}_t + \tilde{\mathcal{A}}\tilde{\mathbf{q}}_z = 0 \quad \text{and} \quad \tilde{\mathcal{A}} = \left(\frac{\partial \tilde{\mathbf{q}}}{\partial \tilde{\mathbf{q}}} \right)^{-1} \mathcal{A} \frac{\partial \tilde{\mathbf{q}}}{\partial \tilde{\mathbf{q}}}, \quad \frac{\partial \tilde{\mathbf{q}}}{\partial \tilde{\mathbf{q}}} = \begin{bmatrix} \bar{\phi}^{-1/2} & 0 & -\frac{1}{2}\bar{\phi}^{-3/2}\tilde{k} \\ 0 & \bar{\phi} & \tilde{a} \\ 0 & 0 & 1 \end{bmatrix}. \quad (4.6)$$

We will be interested in structural properties of the Whitham equations such as hyperbolicity (strict or non-strict), ellipticity and genuine nonlinearity. All of these criteria rely on the eigenvalues c and eigenvectors \mathbf{r} of the Whitham equations that satisfy

$$(\mathcal{A} - c\mathbf{I})\mathbf{r} = 0. \quad (4.7)$$

In general, we expect three eigenpairs $\{(c_j, \mathbf{r}_j)\}_{j=1}^3$ with either all real eigenvalues $c_1 \leq c_2 \leq c_3$ when the Whitham equations are hyperbolic or, in the case of one real and two complex conjugate eigenvalues, the Whitham equations are elliptic. If the eigenvalues are all real and they are strictly ordered $c_1 < c_2 < c_3$, then the Whitham equations are strictly hyperbolic.

The coefficient matrix $\tilde{\mathcal{A}}$ is a similarity transformation of \mathcal{A} , so its eigenvalues are the same. We see that $\tilde{\mathcal{A}}$ exhibits the following property:

$$\tilde{\mathcal{A}}(\tilde{k}, \tilde{a}, \bar{\phi}) = \begin{bmatrix} 1 & 0 & 0 \\ 0 & 1 & 0 \\ 0 & 0 & \bar{\phi} \end{bmatrix} \tilde{\mathcal{A}}(\tilde{k}, \tilde{a}, 1) \begin{bmatrix} \bar{\phi} & 0 & 0 \\ 0 & \bar{\phi} & 0 \\ 0 & 0 & 1 \end{bmatrix}, \quad (4.8)$$

which can be used to show

$$c(\tilde{k}, \tilde{a}, \bar{\phi}) = \bar{\phi} c(\tilde{k}, \tilde{a}, 1), \quad \mathbf{r}(\tilde{k}, \tilde{a}, \bar{\phi}) = \begin{bmatrix} \bar{\phi}^{-1} & 0 & 0 \\ 0 & \bar{\phi}^{-1} & 0 \\ 0 & 0 & 1 \end{bmatrix} \mathbf{r}(\tilde{k}, \tilde{a}, 1). \quad (4.9)$$

Therefore, the hyperbolicity/ellipticity of the Whitham equations is independent of the mean $\bar{\phi}$. The unit mean eigenvalues \tilde{c} and eigenvectors $\tilde{\mathbf{r}}$ are defined according to

$$\tilde{c}(\tilde{k}, \tilde{a}) = c(\tilde{k}, \tilde{a}, 1) \quad \text{and} \quad \tilde{\mathbf{r}}(\tilde{k}, \tilde{a}) = \mathbf{r}(\tilde{k}, \tilde{a}, 1). \quad (4.10)$$

Using the identities in (4.9), we find that the quantity

$$\mu \equiv \nabla_{\tilde{\mathbf{q}}} c(\tilde{k}, \tilde{a}, \bar{\phi}) \cdot \mathbf{r}(\tilde{k}, \tilde{a}, \bar{\phi}) = \begin{bmatrix} \tilde{c}_{\tilde{k}} \\ \tilde{c}_{\tilde{a}} \\ \tilde{c} \end{bmatrix} \cdot \tilde{\mathbf{r}} \quad (4.11)$$

is independent of $\bar{\phi}$, i.e. $\mu = \mu(\bar{k}, \bar{a})$. If $\mu \neq 0$, then the Whitham equations are genuinely nonlinear [2]. For those values of \bar{k} and \bar{a} where $\mu = 0$, the Whitham equations are linearly degenerate. The sign definiteness of μ corresponds to a monotonicity condition that is required for the existence of simple wave solutions to the Whitham equations, of particular importance for the study of DSWs [1].

(a) Weakly nonlinear regime

Now consider equation (4.4) in the small a regime by inserting the Stokes expansion (2.10), (2.11), yielding

$$\mathcal{A} = \begin{bmatrix} \omega_{0,k} & 2a\omega_2 & \frac{\omega_{0,\bar{\phi}}}{2} \frac{4(1 + \bar{\phi}k^2 + 3\bar{\phi}^2k^4 + \bar{\phi}^3k^6)}{(1 + \bar{\phi}k^2)^3} \\ \frac{a}{2}\omega_{0,kk} & \omega_{0,k} & 2\bar{\phi} \\ 0 & 2a\frac{1 - 3\bar{\phi}k^2}{8(1 + \bar{\phi}k^2)} & 2\bar{\phi} \end{bmatrix} + \mathcal{O}(a^2). \quad (4.12)$$

The eigenvalues of \mathcal{A} (characteristic velocities) via (4.9) evaluated at unit mean $\bar{\phi} = 1$ are

$$\left. \begin{aligned} \tilde{c}_1 &= \tilde{\omega}_{0,\bar{k}} - \frac{\tilde{a}}{4}\sqrt{-n\tilde{\omega}_{0,\bar{k}\bar{k}}} + \mathcal{O}(\tilde{a}^2), \\ \tilde{c}_2 &= \tilde{\omega}_{0,\bar{k}} + \frac{\tilde{a}}{4}\sqrt{-n\tilde{\omega}_{0,\bar{k}\bar{k}}} + \mathcal{O}(\tilde{a}^2), \\ \tilde{c}_3 &= 2 + \mathcal{O}(\tilde{a}^2), \end{aligned} \right\} \quad (4.13)$$

and

where $n = n(\bar{k})$ is strictly positive from equation (3.1). The complex characteristic velocities occur precisely when the NLS equation (3.3) is in the focusing regime, i.e. when $\bar{k} > \sqrt{3}$. This is to be expected [2]. The requirement $-n\tilde{\omega}_{0,\bar{k}\bar{k}} > 0$ for modulational stability is sometimes referred to as the Benjamin–Feir–Lighthill criterion [29]. Note that we must use $-n(\bar{k})$, as opposed to $\tilde{\omega}_2(\bar{k})$ from the Stokes expansion (2.9), in the criterion because of the generation of a mean term (cf. [2]).

Next, we determine the approximate eigenvectors $\tilde{\mathbf{r}}_j$ associated with the approximate eigenvalues (4.13) using standard asymptotics of eigenvalues and eigenvectors (e.g. [32]). These approximate results are used to compute μ_j , $j = 1, 2, 3$ (4.11). The expressions are cumbersome, so we do not report them here but there are two noteworthy findings. We find that $\mu_1 = 0$ when

$$\tilde{a} = 6\sqrt{\frac{2}{5}}3^{3/4}(\sqrt{3} - \bar{k})^{3/2} + \mathcal{O}((\sqrt{3} - \bar{k})^{5/2}), \quad 0 < \sqrt{3} - \bar{k} \ll 1. \quad (4.14)$$

Along the curve (4.14), the weakly nonlinear Whitham equations are linearly degenerate in the first characteristic field.

We also find linear degeneracy in the second characteristic field: $\mu_2 = 0$ when $\tilde{a} = 18\bar{k}^2 + \mathcal{O}(\bar{k}^4)$, $0 < \bar{k} \ll 1$. But the weakly nonlinear Whitham equations are non-strictly hyperbolic when $\tilde{a} = 12\bar{k}^2 + \mathcal{O}(\bar{k}^4)$, $0 < \bar{k} \ll 1$, as shown by equating $\tilde{c}_2 = \tilde{c}_3$ from equation (4.13). Because non-strict hyperbolicity implies linear degeneracy [33], there is apparently a contradiction. We argue that this is due to the asymptotic approximations made and the poor accuracy of the approximate periodic wave solution afforded by the Stokes expansion (2.10), (2.11) for small \bar{k} (cf. figures 2 and 3).

(b) Large-amplitude regime

We now investigate modulations of large-amplitude, periodic waves by direct computation of the Whitham equations. For this, we examine the Whitham equations in the form (4.6), so that the dependence on $\bar{\phi}$ is explicit. We numerically compute periodic solutions $\bar{\phi}$ and the corresponding dispersion $\tilde{\omega}(\bar{k}, \bar{a})$ and unit-mean averaging integrals $\{\bar{l}_j(\bar{k}, \bar{a})\}_{j=1}^3$ for the equispaced, discrete values (\bar{k}_j, \bar{a}_l) , $\bar{k}_j = j\Delta$, $\bar{a}_l = l\Delta$, $j, l = 1, 2, \dots, N$. We chose $N = 4000$, $\Delta = 0.001$ so that $\bar{k}_N = \bar{a}_N = 4$.

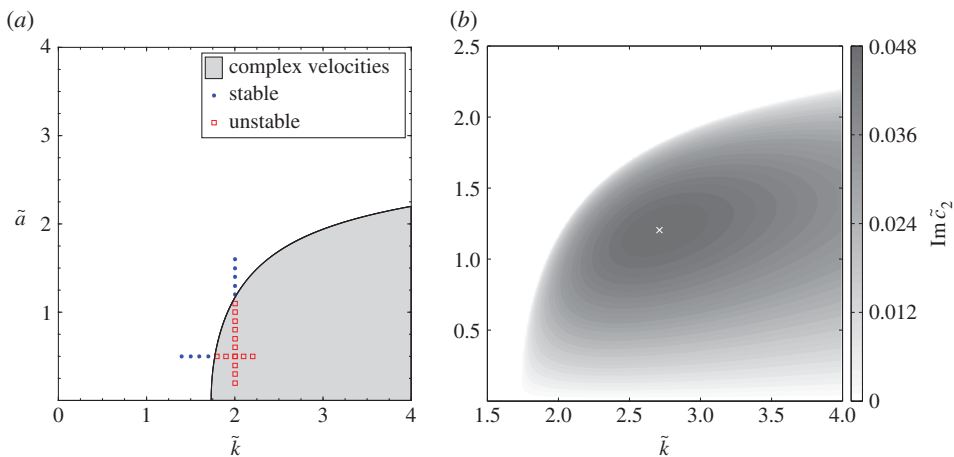


Figure 7. (a) Elliptic (grey) and hyperbolic (white) parameter regimes for the Whitham equations corresponding to complex or real characteristic velocities, respectively. Stable (dots) and unstable (squares) periodic waves according to direct numerical simulation of the conduit equation. (b) Contour plot of the imaginary part of the characteristic velocity \tilde{c}_2 , the approximate MI growth rate. The maximum, 0.04795, occurs for $(\tilde{k}, \tilde{a}) = (2.711, 1.204)$. (Online version in colour.)

Derivatives of $\tilde{\omega}$ and \tilde{l}_j with respect to \tilde{k} and \tilde{a} , required in (4.3), are estimated with sixth-order finite differences, yielding a numerical approximation of the coefficient matrix $\tilde{\mathcal{A}}$ on the discrete grid.

Using our direct computation of the coefficient matrix $\tilde{\mathcal{A}}$, we determine its eigenvalues $\{\tilde{c}_j(\tilde{k}, \tilde{a})\}_{j=1}^3$ and plot in figure 7a the region in the \tilde{k} - \tilde{a} plane where the Whitham equations are hyperbolic or elliptic. The weakly nonlinear analysis (4.13), predicts that the elliptic region appears for $\tilde{k} > \sqrt{3}$, independent of \tilde{a} for small \tilde{a} . But our computations show that the region depends strongly on the wave amplitude.

As noted earlier, ellipticity of the Whitham equations implies modulational instability (MI) of the periodic travelling wave [2]. In agreement with our weakly nonlinear analysis (4.13), we find that, in the elliptic region, $\tilde{c}_1 = \tilde{c}_2^*$ (* denotes complex conjugation) and $\tilde{c}_3 \in \mathbb{R}$. We confirm the hyperbolic/elliptic boundary by direct numerical simulation of the conduit equation (1.1) with slightly perturbed, periodic initial data. Random, smooth noise (band-limited to wavenumber 512) of magnitude $\mathcal{O}(10^{-3})$ was added to a periodic travelling wave initial condition on a domain of over 100 spatial periods. This initial datum was evolved over either 100 temporal periods or to $t = 500$, whichever was longer. Some waves, especially those in the small-amplitude regime, were evolved for even longer time periods. The modulational (in)stability of several of these runs are shown in figure 7a. We find excellent agreement with the MI predictions from Whitham theory. The long-time evolution of two particular waves are shown in figure 8, showing both a stable and an unstable case. The unstable case in figure 8b appears to show the formation of large-amplitude, bright envelope coherent structures. This is additional numerical evidence for the existence of bright envelope soliton solutions of the conduit equation.

A periodic travelling wave solution of the conduit equation (1.1) corresponds to a constant solution $\tilde{\mathbf{q}}(z, t) = \tilde{\mathbf{q}}_0$ of the Whitham equations (4.6). If we consider the stability of this solution by linearizing the Whitham equations according to $\tilde{\mathbf{q}}(z, t) = \tilde{\mathbf{q}}_0 + \mathbf{b}e^{i\kappa z + \sigma t}$, $|\mathbf{b}| \ll 1$, we obtain the growth rates

$$\text{Re } \sigma_i = \kappa \text{Im } c_i \quad (4.15)$$

for each component of the perturbation in the eigenvector basis of $\tilde{\mathcal{A}}$. The physical growth rate requires knowledge of the wavenumber κ . Because the Whitham equations are quasi-linear, first-order equations, any wavenumber is permissible (determined by the initial data), suggesting that the physical growth rate (4.15) is unbounded. In practice, there is a dominant wavenumber

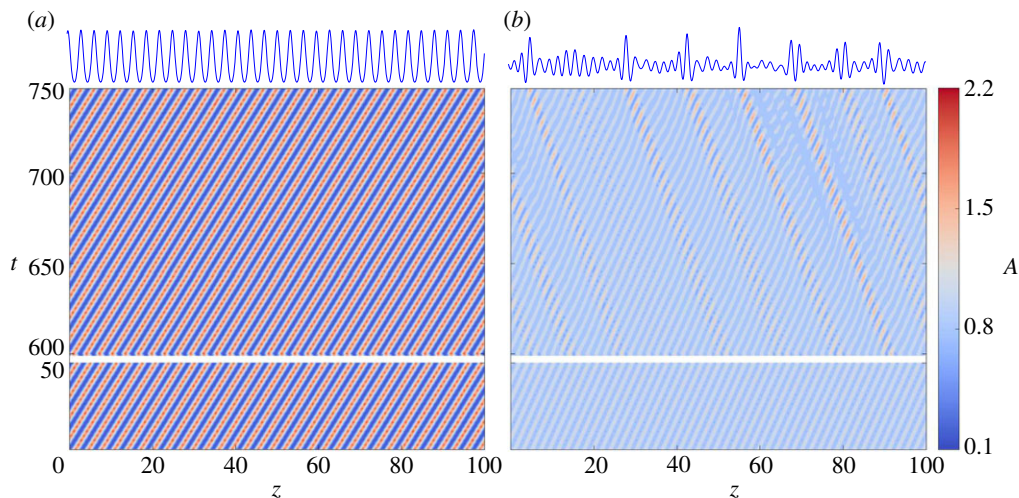


Figure 8. Numerical evolution of perturbed periodic wave solutions in the conduit equation. (a) Modulationally stable case: $(\tilde{k}, \tilde{a}) = (2, 2)$. (b) Modulationally unstable case: $(\tilde{k}, \tilde{a}) = (3, 0.5)$. Top: the respective cases at the final time $t = 750$. (Online version in colour.)

associated with the instability that is determined by higher order effects, which in this case would be higher order dispersion in the Whitham equations. The NLS equation (3.3) resolves this feature in the weakly nonlinear regime, but we are interested in large-amplitude modulations. We therefore identify the imaginary part of the characteristic velocity \tilde{c}_2 as a proxy for the growth rate of the instability and observe in figure 7b that there is a maximum of $\text{Im}(\tilde{c}_2)$ for unit-mean periodic waves that occurs for the wave parameters $(\tilde{k}, \tilde{a}) = (2.711, 1.204)$. We confirm that these parameters do indeed approximately correspond to a maximally unstable periodic wave by performing numerical simulations of the conduit equation (1.1) with initially perturbed periodic travelling waves, using the same process as that used in the determination of modulational (in)stability. The envelopes of these waves were extracted for each time step and then compared to the envelope of the initial condition, giving a deviation from the expected periodic wave evolution. The growth rate was calculated by fitting an exponential to the maximum of this deviation. From these numerics, the maximally unstable parameters are closer to $(\tilde{k}, \tilde{a}) = (2.7, 1.35)$ than the expected $(\tilde{k}, \tilde{a}) = (2.7, 1.2)$. The maximal growth rate for these parameters was found to be 0.0457, which is within 5% of the maximal growth rate found via the Whitham equations if we assume a unit perturbation wavenumber κ in (4.15).

Next, we compute the quantities $\{\mu_j(\tilde{k}, \tilde{a})\}_{j=1}^3$ from equation (4.11) on the discrete grid $\{(\tilde{k}_j, \tilde{a}_l)\}_{j,l=1}^N$ using sixth-order finite differencing. The results are depicted in figure 9a where the curves correspond to the largest value of \tilde{k} , given \tilde{a} , such that μ changes sign. The curve where μ_1 changes sign bifurcates from the edge of the elliptic region at the point $(\tilde{k}, \tilde{a}) = (\sqrt{3}, 0)$, agreeing with the weakly nonlinear result (4.14) for sufficiently small \tilde{a} . The curve where both $\mu_{2,3}$ change sign apparently bifurcates from $(0, 0)$ and occurs for small \tilde{k} . These results demonstrate that the Whitham equations lack genuine nonlinearity when considered in the whole of the hyperbolic region.

To understand the small \tilde{k} results better, we show in figure 9b a zoom-in of this region. The accurate determination of the loss of genuine nonlinearity in this region is numerically challenging because the characteristic velocities $\tilde{c}_{2,3}$ get very close to one another. A more numerically stable calculation is shown by the black dashed curve in figure 9b where, for each \tilde{a} , it corresponds to the largest \tilde{k} at which $|\tilde{c}_3 - \tilde{c}_2| < 10^{-5}$. For parameters to the left of this curve, the characteristic velocities remain very close to one another. It is well-known that, for example, in the

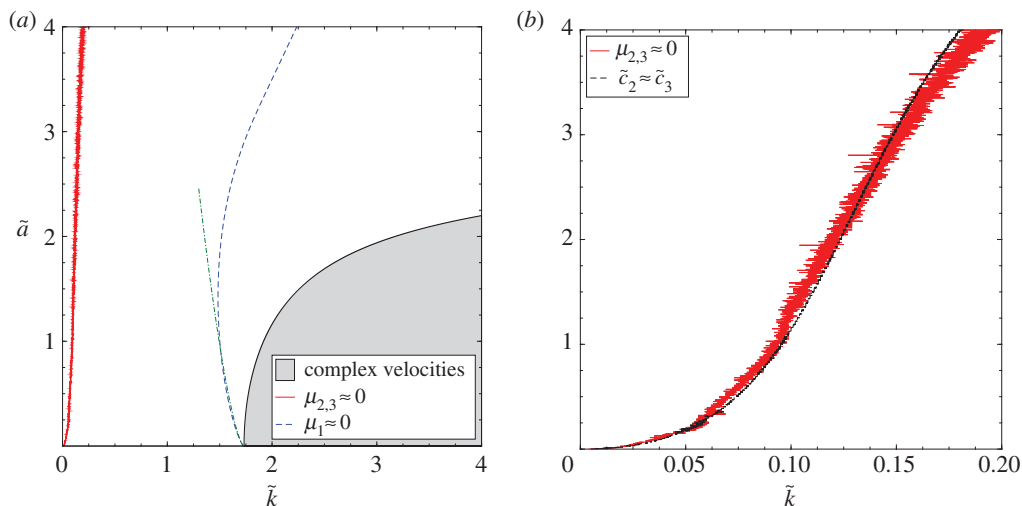


Figure 9. (a) Loss of genuine nonlinearity in the Whitham equations. The curves correspond to regions in the \tilde{k} - \tilde{a} plane where the computed quantities $\mu_{2,3}$ (solid) or μ_1 (dashed) change sign. To the right of the solid (dashed) curve, $\mu_3 > 0$, $\mu_2 < 0$ ($\mu_1 > 0$). The dashed-dotted curve corresponds to the prediction $\mu_1 = 0$ from a weakly nonlinear analysis. The elliptic region from figure 7 is also depicted (grey). (b) Zoom-in of the small \tilde{k} region of (a) where $\mu_{2,3} \approx 0$ (solid, noisy) approximately corresponds to the largest \tilde{k} , to the left of which $|\tilde{c}_3 - \tilde{c}_2| < 10^{-5}$ (dashed, smooth), i.e. approaching non-strict hyperbolicity. (Online version in colour.)

KdV Whitham equations, the characteristic velocities get exponentially close to one another, yet remain distinct in the small wavenumber regime [34,35]. Because non-strict hyperbolicity implies loss of genuine nonlinearity [33], the proximity of \tilde{c}_2 and \tilde{c}_3 may be affecting the numerical results. It remains to definitively determine if the Whitham equations lose strict hyperbolicity and/or genuine nonlinearity in the small \tilde{k} regime. Note that the curve for which $\mu_1 = 0$ in figure 9a occurs in a strictly hyperbolic region.

5. Discussion/conclusion

Our study of the structural properties of the conduit Whitham equations sheds some light on recent theoretical and experimental studies of dispersive shock waves. The DSW fitting method allows one to determine a dispersive shock's harmonic and soliton edge speeds, even for non-integrable systems [36]. However, the method is known to break down when the Whitham equations lose genuine nonlinearity in the second characteristic field [1,26]. It was observed in [26] that the fitting method failed to accurately predict conduit DSW soliton edge speeds for sufficiently large jump heights. Our results here suggest that this could be due to the loss of strict hyperbolicity and/or genuine nonlinearity in the small wavenumber (soliton train) regime.

In addition to the hyperbolic modulation regime where DSWs and dark envelope solitons are prominent coherent structures, we have found an elliptic regime where the periodic wave breaks up into coherent wave-packets or bright envelope solitons. The accessibility of both hyperbolic and elliptic modulation regimes in one system motivates further study of each and the transition between the two. One potential future, novel direction is to explore the possibility of creating a soliton gas [37].

It remains to generate a periodic wave from an initially uniform conduit and explore its properties experimentally. Accurate control of wave-breaking via a dispersionless simple wave (a rarefaction wave) has been achieved by slow modulation of the conduit area from a boundary [11]. One generalization of this is to use simple wave solutions of the Whitham equations to efficiently and smoothly transition between a constant conduit $\tilde{a} = 0$ to a periodic conduit $\tilde{a} > 0$.

This also suggests the theoretical and experimental exploration of Riemann problems, step initial data, for the Whitham equations themselves. Our determination of linearly degenerate curves will inform the ability to construct simple waves connecting two generic wave states.

We have presented strong numerical evidence for the existence of large-amplitude dark and bright envelope solitary waves in viscous fluid conduits, bifurcating from weakly nonlinear NLS solutions. Dark envelope solitons can have either positive or negative velocities. All bright envelope solitons for NLS have negative velocities. It remains to be determined if this is the case in the large-amplitude case. Existing laboratory studies of viscous fluid conduits implement control of the conduit interface by varying the injected flow rate through a nozzle at the bottom of a fluid column. This allows for the creation of waves with positive (upward) propagation velocities such as dark envelope solitons. If bright envelope solitons only have negative velocities, then an alternative experimental approach will be required to create them.

We have shown that the non-convexity of the conduit linear dispersion relation leads to the existence of elliptic Whitham equations and modulational instability. This is just one possible implication of non-convex dispersion in dispersive hydrodynamics. We note that non-convex dispersion in other, higher order equations has also been found to give rise to a resonance between the DSW soliton edge and linear waves, leading to the generation of radiating DSWs [38–40].

This study has identified and categorized modulations of both small- and large-amplitude periodic travelling waves for the conduit equation (1.1). These findings, along with previous theoretical and experimental studies of solitons and DSWs in the strongly nonlinear regime imply that the viscous fluid conduit system is an accessible environment in which to investigate rich and diverse nonlinear wave phenomena.

Data accessibility. This paper contains no experimental data. All computational results are reproducible.

Authors' contributions. Both authors contributed equally to problem formulation, solution and writing of the paper.

Competing interests. We have no competing interests.

Funding. This work was partially supported by NSF CAREER DMS-1255422 (M.A.H.) and NSF GRFP (M.D.M.).

Appendix A. Numerical methods

(a) Periodic solutions

We compute unit-mean conduit periodic travelling wave solutions $\tilde{\phi}(\theta)$ for specified (\tilde{k}, \tilde{a}) with a Newton-GMRES iterative method [41] on the first integral of equation (2.1)

$$A + \tilde{\omega}\tilde{\phi} - \tilde{k}\tilde{\phi}^2 - \tilde{\omega}\tilde{k}^2\tilde{\phi}\tilde{\phi}'' + \tilde{\omega}\tilde{k}^2(\tilde{\phi}')^2 = 0, \quad (\text{A } 1)$$

where $A \in \mathbb{R}$ is an integration constant. We use a spectral method to compute the unit-mean cosine series representation $\tilde{\phi}(\theta) = 1 + \sum_{n=1}^N 2a_n \cos n\theta$. Equation (A 1) is discretized in spectral space $\{a_n\}_{n=1}^N$ with the fast and accurate computation of derivatives achieved via fast cosine transforms (DCT II in [42]). The projection of (A 1) onto constants determines A , which we do not require because of our imposition of unit mean. Projection of equation (A 1) onto $\cos(n\theta)$ for $n = 1, \dots, N$ yields N equations for the $N + 1$ unknowns $(\{a_n\}_{n=1}^N, \tilde{\omega})$. The amplitude constraint $\tilde{\phi}(\pi) - \tilde{\phi}(0) = -4 \sum_{n \text{ odd}} a_n = \tilde{a}$ closes the system of equations. We precondition the spectral equations by dividing each by the sum of linear coefficients, shifted by $2k + 1$, i.e. by $\tilde{\omega} + n^2 \tilde{\omega} \tilde{k}^2 + 1$. The accurate resolution of each solution is maintained by achieving an absolute tolerance of 10^{-13} in the 2-norm of the residual and choosing N so that $|a_n|$ is below $5 \cdot 10^{-12}$ for $n > 3N/4$. The number of coefficients required strongly depends on the wavenumber \tilde{k} . For example, when $0.5 \leq \tilde{k} \leq 4$, we find $N = 2^6$ provides sufficient accuracy, whereas for $0.002 \leq \tilde{k} \leq 0.01$, approaching the soliton limit $\tilde{k} = 0$ we use $N = 2^{12}$.

With the cosine series coefficients of $\tilde{\phi}(\theta)$ in hand, we compute the unit-mean averaging integrals $\tilde{I}_j, j = 1, 2, 3$ in equations (4.5), (4.2) using the spectrally accurate trapezoidal rule. We then use sixth-order finite differencing to compute derivatives of \tilde{I}_j and $\tilde{\omega}$ on a grid of wavenumbers

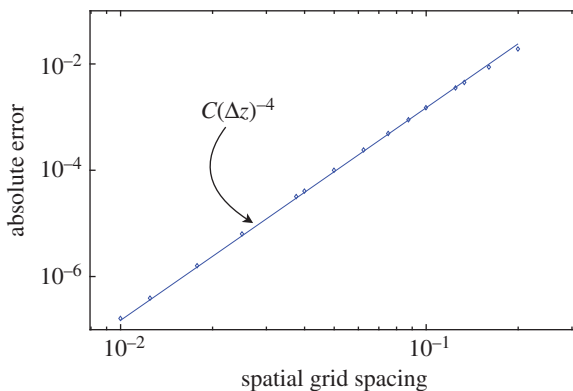


Figure 10. Maximum absolute error in the direct numerical simulation of the conduit equation, achieving fourth-order spatial accuracy as expected. The solution used in validation was a periodic wave with $k = 3$ and $a = 0.5$ generated with accuracy 10^{-8} , and was simulated over 50 spatial periods and five temporal periods. The reference line is $C(\Delta z)^{-4}$. (Online version in colour.)

and amplitudes as explained in §4b. This numerically determines the Whitham equations in the form (4.6).

(b) Time-stepping

For the direct numerical simulation of the conduit equation (1.1), it is convenient to write it in the form of two coupled equations:

$$\left. \begin{aligned} A_t &= A\mathcal{P} \\ \text{and} \quad A\mathcal{P} + (A^2)_z - (A^2\mathcal{P}_z)_z &= 0. \end{aligned} \right\} \quad (\text{A } 2)$$

The first equation is a temporal ODE in time and the second equation is a linear, elliptic problem $\mathcal{L}(A)\mathcal{P} = -(A^2)_z$ in space. We solve for \mathcal{P} using an equispaced fourth-order finite difference discretization and direct inversion of the resulting banded linear system. We implement time-dependent boundary conditions with prescribed $A(0, t)$ and $A(L, t)$ so that the first equation in (A 2) yields the boundary conditions for \mathcal{P} . Time-stepping is achieved with a fourth-order, explicit Runge–Kutta method with variable time-step (MATLAB’s ode45). The solver was validated against computed periodic travelling wave solutions from the previous subsection. The maximum error between the numerical solution and the periodic travelling wave solution is reported in figure 10, demonstrating fourth-order spatial convergence.

Appendix B. Nonlinear Schrödinger equation derivation

Here, we derive an approximation of wave modulations in the small-amplitude, weakly nonlinear regime. Consider the ansatz

$$A(z, t) = 1 + \varepsilon A_0 + \varepsilon^2 A_1 + \varepsilon^3 A_2 + \dots, \quad \varepsilon \rightarrow 0, \quad (\text{B } 1)$$

where $A_i = A_i(\theta, Z, T)$ for $i = 0, 1, \dots$, $\theta = \tilde{k}z - \tilde{\omega}_0(\tilde{k})t$, $Z = \varepsilon z$ and $T = \varepsilon t$, where $\tilde{\omega}_0(\tilde{k})$ is the linear dispersion relation (1.5) for unit mean. Then, at $\mathcal{O}(\varepsilon)$, we obtain a linear, homogeneous equation for A_0 : $\mathcal{L}A_0 := -\omega A_{0,\theta} + 2kA_{0,\theta} + k^2\omega A_{0,3\theta} = 0$, with solution $A_0 = \psi(Z, T)e^{i\theta} + \text{c.c.}$, where ‘c.c.’ denotes the complex conjugate of the previous terms. At $\mathcal{O}(\varepsilon^2)$, $\mathcal{L}A_1 = F_1$, where

$$F_1 = e^{2i\theta}[-2i\tilde{k}\psi^2] + e^{i\theta}[-\psi_T - \tilde{k}^2\psi_T - 2\psi_Z + 2\tilde{k}\tilde{\omega}_0\psi_Z] + \text{c.c.}$$

Solvability therefore implies $-(1 + \tilde{k}^2)[\psi_T + \tilde{\omega}'_0(k)\psi_Z] \sim \varepsilon g_1 + \dots$, where we have introduced the higher order correction g_1 . Solving for A_1 , we include second harmonic and mean terms $A_1 = \psi^2(Z, T) e^{2i\theta} / (3\tilde{k}\tilde{\omega}) + \text{c.c.} + M(Z, T)$ with M to be determined at the next order. Solvability with respect to constants at $\mathcal{O}(\varepsilon^3)$ yields $M = (3\tilde{k} - 1)(1 + \tilde{k}^2)\tilde{k}^{-2}(\tilde{k}^2 + 3)^{-1}|\psi|^2$. Solvability with respect to the first harmonic yields g_1 , which, upon entering the moving reference frame and scaling to long time $\xi = Z - \tilde{\omega}'_0 T$, $\tau = \varepsilon T$, yields the NLS equation in the form

$$i\psi_\tau + \frac{\tilde{\omega}''(\tilde{k})}{2} \psi_{\xi\xi} + \frac{3 + 5\tilde{k}^2 + 8\tilde{k}^4}{3\tilde{k}(\tilde{k}^2 + 1)(\tilde{k}^2 + 3)} |\psi|^2 \psi = 0. \quad (\text{B2})$$

Rescaling according to (3.2) and $B = \psi / \sqrt{n}$ yields the NLS equation (3.3).

Appendix C. Derivation of the Whitham equations

For completeness, we supply a synopsis of the multiple scales asymptotic derivation of the Whitham modulation equations. For the formal derivation here, we introduce slow space and time scales $Z = \varepsilon z$, $T = \varepsilon t$ and consider the ansatz $A(z, t) = A_0(\theta, Z, T) + \varepsilon A_1(\theta, Z, T) + \dots$, $0 < \varepsilon \ll 1$, where $\theta_z = k$ and $\theta_t = -\omega$. Continuity of mixed partials $\theta_{zt} = \theta_{tz}$ implies the conservation of waves $k_T + \omega_Z = 0$, one of the Whitham equations. We insert the asymptotic ansatz into the conduit equation (1.1) and equate like orders in ε . The $\mathcal{O}(1)$ equation is

$$-\omega A_{0,\theta} + 2k A_0 A_{0,\theta} - k^2 \omega A_{0,\theta} A_{0,\theta\theta} + k^2 \omega A_0 A_{0,\theta\theta\theta} = 0. \quad (\text{C1})$$

The above equation is solved with a family of periodic travelling waves parametrized by $(k, a, \bar{\phi})$ (see §2) where the parameters are assumed to depend on the slow variables (Z, T) . Note that in order to remove secularities at this order, the period of the solution must be scaled to a constant [2,31], which we choose to be 2π without loss of generality.

At the next order, $\mathcal{O}(\varepsilon)$, we obtain the linear problem $\mathcal{L}A_1 = f$ where

$$\mathcal{L}A_1 = -\omega A_{1,\theta} + (-k^2 \omega A_{0,\theta} A_{1,\theta} + 2k A_0 A_{1,\theta}) + k^2 \omega (A_{1,\theta\theta\theta} A_0 + A_{0,\theta\theta\theta} A_1)$$

and

$$f = -A_{0,T} - k^2 A_{0,\theta\theta} A_{0,T} + k^2 A_0 A_{0,\theta\theta T} - 2A_0 A_{0,Z} + 2k \omega A_{0,\theta} A_{0,\theta Z} - 2k \omega A_0 A_{0,\theta\theta Z}.$$

There are two solvability conditions in the form $\langle w, f \rangle \equiv \int_0^{2\pi} w(\theta) f(\theta) d\theta = 0$, where $w \in \text{Ker } \mathcal{L}^* = \text{span}\{1, A_0^{-2}\}$ for the adjoint operator

$$\mathcal{L}^* w = \omega w_\theta + k^2 \omega [-(A_{0,\theta} w)_{\theta\theta} + (A_{0,\theta\theta} w)_\theta + A_{0,3\theta} w - (A_0 w)_{3\theta}] + 2k [A_{0,\theta} w - (A_0 w)_\theta],$$

with 2π -periodic boundary conditions. Note that there is a third, linearly independent function that is annihilated by \mathcal{L}^* , but it is not 2π -periodic. Applying the two solvability conditions $\langle 1, f \rangle = \langle A_0^{-2}, f \rangle = 0$, and adding the conservation of waves, we arrive at the Whitham equations

$$(\overline{A_0})_T + (\overline{A_0^2} - 2k\omega \overline{A_{0,\theta}^2})_Z = 0, \quad (\text{C2})$$

$$\left(\frac{\overline{I}}{\overline{A_0}} + k^2 \frac{\overline{A_{0,\theta}^2}}{\overline{A_0^2}} \right)_T - 2 \left(\overline{\ln A_0} \right)_Z = 0 \quad (\text{C3})$$

and

$$k_T + \omega_Z = 0, \quad (\text{C4})$$

where $\bar{g} = \langle 1, g \rangle$. Setting $\varepsilon = 1$, i.e. considering the Whitham equations as the long time $t \gg 1$ asymptotic, we obtain equations (4.1).

Averaging of the conservation laws (1.3) is achieved by inserting the ansatz $A(z, t) = \phi(\theta)$ and averaging the densities and fluxes over a period:

$$\bar{\phi}_t + \overline{(\phi^2 + \omega k \phi^2 (\phi^{-1} \phi_\theta)_\theta)}_z = 0$$

and

$$\left(\frac{1}{\phi} + k^2 \frac{\phi_\theta^2}{\phi^2} \right)_t + \left(-\omega k \frac{\phi_{\theta\theta}}{\phi} + \omega k \frac{\phi_\theta \phi_\theta}{\phi^2} - 2 \ln \phi \right)_z = 0.$$

Integration by parts and the addition of conservation of waves yields the same set of Whitham equations (4.1).

References

1. El GA, Hoefler MA. 2016 Dispersive shock waves and modulation theory. *Physica D* **333**, 11–65. (doi:10.1016/j.physd.2016.04.006)
2. Whitham GB. 1974 *Linear and nonlinear waves*. New York, NY: Wiley.
3. Scott DR, Stevenson DJ, Whitehead JA. 1986 Observations of solitary waves in a viscously deformable pipe. *Nature* **319**, 759–761. (doi:10.1038/319759a0)
4. Lowman NK, Hoefler MA. 2013 Dispersive hydrodynamics in viscous fluid conduits. *Phys. Rev. E* **88**, 23016. (doi:10.1103/PhysRevE.88.023016)
5. Harris SE, Clarkson PA. 2006 Painleve analysis and similarity reductions for the magma equation. *SIGMA* **2**, 068. (doi:10.3842/SIGMA.2006.068)
6. Olson P, Christensen U. 1986 Solitary wave propagation in a fluid conduit within a viscous matrix. *J. Geophys. Res.* **91**, 6367–6374. (doi:10.1029/JB091iB06p06367)
7. Whitehead JA, Helfrich KR. 1990 Magma waves and diapiric dynamics. In *Magma transport and storage* (ed. MP Ryan), pp. 53–76. Chichester, UK: John Wiley & Sons.
8. Helfrich KR, Whitehead JA. 1990 Solitary waves on conduits of buoyant fluid in a more viscous fluid. *Geophys. Astro. Fluid* **51**, 35–52. (doi:10.1080/03091929008219850)
9. Whitehead JA, Helfrich KR. 1988 Wave transport of deep mantle material. *Nature* **336**, 59–61. (doi:10.1038/336059a0)
10. Lowman NK, Hoefler MA, El GA. 2014 Interactions of large amplitude solitary waves in viscous fluid conduits. *J. Fluid Mech.* **750**, 372–384. (doi:10.1017/jfm.2014.273)
11. Maiden MD, Lowman NK, Anderson DV, Schubert ME, Hoefler MA. 2016 Observation of dispersive shock waves, solitons, and their interactions in viscous fluid conduits. *Phys. Rev. Lett.* **116**, 174501. (doi:10.1103/PhysRevLett.116.174501)
12. Whitehead JA, Luther DS. 1975 Dynamics of laboratory diapir and plume models. *J. Geophys. Res.* **80**, 705–717. (doi:10.1029/JB080i005p00705)
13. McKenzie D. 1984 Generation and compaction of partially molten rock. *J. Petrology* **25**, 713–765. (doi:10.1093/petrology/25.3.713)
14. Richter FM, McKenzie D. 1984 Dynamical models for melt segregation from a deformable matrix. *J. Geol.* **92**, 729–740. (doi:10.1086/628908)
15. Simpson G, Spiegelman M, Weinstein MI. 2010 A multiscale model of partial melts 1: effective equations. *J. Geophys. Res.* **115**, B04410. (doi:10.1029/2009JB006375)
16. Lax PD. 1968 Integrals of nonlinear equations of evolution and solitary waves. *Comm. Pur. Appl. Math.* **21**, 467–490. (doi:10.1002/cpa.3160210503)
17. Barcilon V, Richter FM. 1986 Nonlinear waves in compacting media. *J. Fluid Mech.* **164**, 429–448. Digital Archive. (doi:10.1017/S0022112086002628)
18. Harris S. 1996 Conservation laws for a nonlinear wave equation. *Nonlinearity* **9**, 187–208. (doi:10.1088/0951-7715/9/1/006)
19. Simpson G, Spiegelman M, Weinstein MI. 2007 Degenerate dispersive equations arising in the study of magma dynamics. *Nonlinearity* **20**, 21–49. (doi:10.1088/0951-7715/20/1/003)
20. Scott DR, Stevenson DJ. 1984 Magma solitons. *Geophys. Res. Lett.* **11**, 1161–1164. (doi:10.1029/GL011i011p01161)
21. Nakayama M, Mason DP. 1991 Compressive solitary waves in compacting media. *Int. J. Nonlin. Mech.* **26**, 631–640. (doi:10.1016/0020-7462(91)90015-L)
22. Simpson G, Weinstein M. 2008 Asymptotic stability of ascending solitary magma waves. *SIAM J. Math. Anal.* **40**, 1337–1391. (doi:10.1137/080712271)

23. Whitehead JA, Helfrich KR. 1986 The Korteweg–deVries equation from laboratory conduit and magma migration equations. *Geophys. Res. Lett.* **13**, 545–546. (doi:10.1029/GL013i006p00545)
24. Marchant TR, Smyth NF. 2005 Approximate solutions for magmon propagation from a reservoir. *IMA J. Appl. Math.* **70**, 796–813. (doi:10.1093/imamat/hxh069)
25. Elperin T, Kleeorin N, Krylov A. 1994 Nondissipative shock waves in two-phase flows. *Physica D* **74**, 372–385. (doi:10.1016/0167-2789(94)90201-1)
26. Lowman NK, Hoefer MA. 2013 Dispersive shock waves in viscously deformable media. *J. Fluid Mech.* **718**, 524–557. (doi:10.1017/jfm.2012.628)
27. Whitham GB. 1965 A general approach to linear and non-linear dispersive waves using a Lagrangian. *J. Fluid Mech.* **22**, 273–283. (doi:10.1017/S0022112065000745)
28. Ablowitz MJ. 2011 *Nonlinear dispersive waves: asymptotic analysis and solitons*, 1st edn. Cambridge, UK: Cambridge University Press.
29. Zakharov VE, Ostrovsky LA. 2009 Modulation instability: the beginning. *Physica D* **238**, 540–548. (doi:10.1016/j.physd.2008.12.002)
30. Whitham GB. 1965 Non-linear dispersive waves. *Proc. R. Soc. A* **283**, 238–261. (doi:10.1098/rspa.1965.0019)
31. Luke JC. 1966 A perturbation method for nonlinear dispersive wave problems. *Proc. R. Soc. Lond. A* **292**, 403–412. (doi:10.1098/rspa.1966.0142)
32. Hinch EG. 1991 *Perturbation methods*. Cambridge, UK: Cambridge University Press.
33. Dafermos CM. 2009 *Hyperbolic conservation laws in continuum physics*, 3rd edn. Berlin, Germany: Springer.
34. Levermore D. 1988 The hyperbolic nature of the zero dispersion KdV limit. *Commun. Part Diff. Equ.* **13**, 495–514. (doi:10.1080/03605308808820550)
35. Gurevich AV, Krylov AL, El GA. 1990 Nonlinear modulated waves in dispersive hydrodynamics. *Sov. Phys. JETP* **71**, 899–910.
36. El GA. 2005 Resolution of a shock in hyperbolic systems modified by weak dispersion. *Chaos* **15**, 37103. (doi:10.1063/1.1947120)
37. El GA, Kamchatnov AM. 2005 Kinetic equation for a dense soliton gas. *Phys. Rev. Lett.* **95**, 204101. (doi:10.1103/PhysRevLett.95.204101)
38. Conforti M, Baronio F, Trillo S. 2014 Resonant radiation shed by dispersive shock waves. *Phys. Rev. A* **89**, 13807. (doi:10.1103/PhysRevA.89.013807)
39. El GA, Smyth NF. 2016 Radiating dispersive shock waves in non-local optical media. *Proc. R. Soc. A* **472**, 20150633. (doi:10.1098/rspa.2015.0633)
40. Sprenger P, Hoefer MA. In press. Shock waves in non-convex dispersive hydrodynamics. *SIAM J. Appl. Math.* (<http://arxiv.org/abs/1606.09229>).
41. Kelley CT. 1995 *Iterative methods for linear and nonlinear equations*. Philadelphia, PA: SIAM.
42. Wang Z, Hunt BR. 1985 The discreteW transform. *Appl. Math. Comput.* **16**, 19–48. (doi:10.1016/0096-3003(85)90008-6)